JOURNAL OF MATERIALS SCIENCE 37 (2002) 895–904

Investigation of time-dependent characteristics of materials and micromechanisms of plastic deformation on a submicron scale by a new pulse indentation technique

YU. I. GOLOVIN, A. I. TYURIN, B.YA. FARBER*,‡
Department of Physics, Tambov State University, Tambov, Russia
E-mail: golovin@tsu.tmb.ru; ygolovin@inbox.ru; bfarber@zircoa.com

A new pulse technique is proposed to investigate dynamics and micromechanisms of plastic deformations of materials underneath the indenter during microindentation. It is established that the process of indenter penetration under pulse loading conditions can be described by several distinct stages (as many as four in some cases) differing in kinetics and activation parameters. In each investigated material, the first stage was characterized by a high strain rate ($\geq 10^3$ s^{-1}) and the high contact stresses (dynamic hardness), which exceeded static hardness by factor of 5–10. Typical values of activation volumes during the first stage were of the order of 10^{-30} m^3 , i.e. close to the volume occupied by an atom (ion) in a lattice. During the second and the subsequent stages, the activation volume in ionic crystals increased up to about 10^{-28} m^3,(i.e. $10b^3$, where b is Burger's vector of glide dislocations). Dynamics of initial stages of the indenter penetration was, therefore, determined by elastic and subsequently by plastic deformation, which is carried out by non-equilibrium point defects (most likely by interstitials or crowdions). A relative role of point defects in the process of mass transfer underneath the indenter and its contribution to microhardness is estimated. In soft materials (NaCl, LiF, Pb) during long indentation times ($\geq$1 s) contribution of point defects can be estimated as more than 10%, and in the case of hard materials (Si, amorphous alloys) became closer to 100%. Dynamics of the final stages of the indenter penetration in soft crystals were governed by the dislocation creep. In all investigated materials for short indentation times ($\ll$1 s) plastic deformation underneath the indenter occurred predominantly via generation and motion of interstitials and their clusters containing a few atoms.

1. Introduction

Dynamic, time-dependent material properties, the spectrum of generated structural defects and atomic material-transfer mechanisms during collisions of solids are extremely important for understanding the nature of surface damage and hardening, grinding, milling, mechanical activation of chemical reactions and mechanical alloying, abrasive wear, and so on.

Hardness test -a traditional method for express investigation of the mechanical properties of solids (in particular, thin films and sub-surface layers) involves measurements of the residual impression size left on a sample surface by a hard indenter. A significant improvement in the capabilities of hardness testing is attributed to depth-sensing technique, proposed in the early seventies [1]. Controllable penetration of the indenter and continuous recording of the resistance force, F, as a function of the penetration depth, h, made it possible to localize zone under study within few nm^3 [2–7]. So far, primary application of the nanoindentation method was measurements of the macroscopical material's properties (such as hardness and modulus of elasticity). High measurement accuracy requires high force and spatial resolution, which were achieved in nanoindentation by relatively slow (quasi-equilibrium) loading and unloading (the whole cycle conventionally takes about a minute). Low time resolution of the traditional nanoindentation method significantly limits its capabilities to study very early stages of the indenter penetration into the material, which is very important for understanding mechanisms of point defect generation during indentation.

There are many papers devoted to kinetics investigation of the last slow stages of the penetration during

*Author to whom all correspondence should be addressed.
‡*Present Address*: Zircoa, Inc., 31501 Solon Road, Solon, OH 44139, USA.

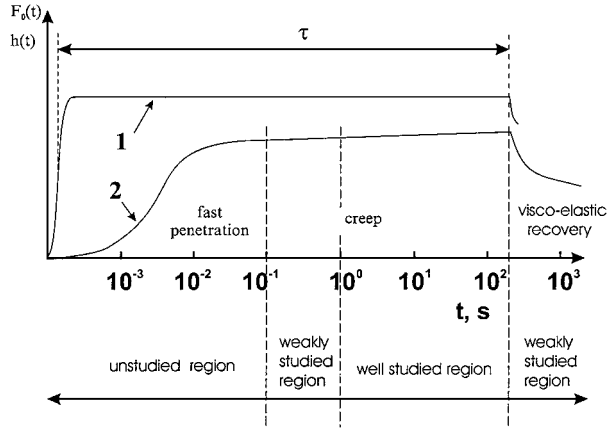

Figure 1 A schematic diagram for measurements of time-dependent characteristics of materials by fast displacement sensitive indentation. 1: "rectangular" load pulse $F_0(t)$; 2: indenter penetration depth $h(t)$.

creep regime, with the size of the residual impression being changed within several percent during a period of $10^2 \div 10^3$ s (see for example [8–11]).

Kinetics of the fast indenter penetration has been described in [12, 13]. However, the time resolution in these works was too low to study the most interesting initial stages of the indenter penetration.

It is well known that the simplest and the most comprehensive way to investigate dynamical properties of a system is to analyze its response to a quasi-instantaneous excitation. In our work, we have employed this approach to study indentation process by applying an "instantaneous" test load to the indenter and continuously recording kinetics of its penetration into the material with an adequate time resolution (Fig. 1). The penetration kinetics in this case is determined exclusively by dynamic properties of the material and structural defects in it, provided that the penetration starts with zero initial velocity (at the initial position, the indenter slightly touches the surface of the specimen). As a result, it becomes feasible to analyze continuously *in situ* the deformation velocity as a function of the instantaneous contact stresses, and to distinguish various stages of the process, and to subject them to thermoactivation analysis. The magnitudes of an activation energy and activation volume allow in turn to understand the micro-mechanisms of mass transfer underneath the indenter. In other words, studying time dependent characteristics of solids make it possible not only to measure a dynamic hardness, H_d, but also to understand the nature of microhardness in connection with basic physical processes of nucleation and motion of certain structural defects.

In this paper we describe a new technique for investigation of the dynamics of the residual impression formation with a spatial resolution of 1 nm and time resolution of 50 μs. We were also able to investigate electrical processes [14, 15] accompanying indentation with a time resolution of 0.1 μs. The results obtained for single crystals of Si, MgO, LiF, NaCl, KCl, Pb, Al with various impurity contents and for some amorphous alloys in a temperature range 77–293 K are analyzed in terms of dynamics and mass transfer micromechanisms underneath the indenter [16, 17].

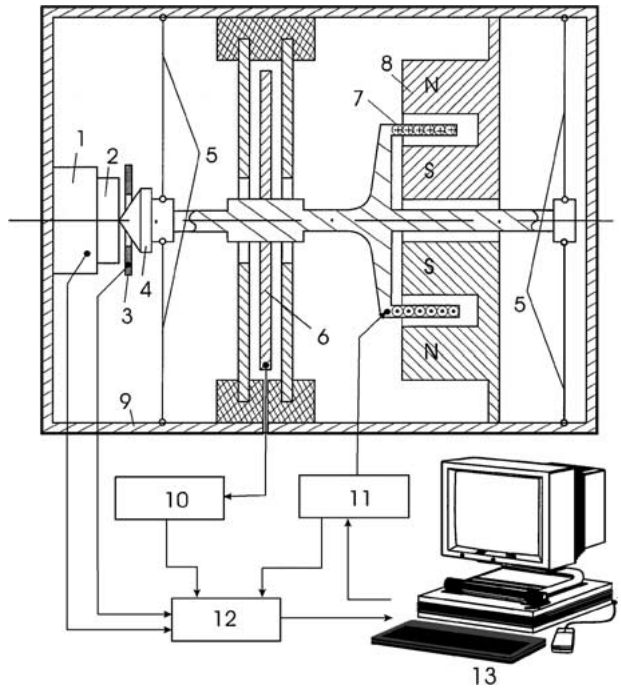

Figure 2 A schematic diagram of experimental tester: 1: piezo - gauge; 2: sample; 3: antenna; 4: indenter; 5: suspension diaphragm; 6: capacitance displacement gauge; 7: movable coil; 8: permanent magnet; 9: shield; 10: capacitive displacement gauge amplifier; 11: function generator; 12: data acquisition system; 13: computer.

2. Experimental technique

The apparatus contained a horizontal shaft mounted on two soft flat springs for frictionless straight displacement (Fig. 2). The Berkovich diamond pyramid indenter was mounted on the left end of the shaft and an electromagnetic force transducer was attached to the right hand side of the shaft. A micrometer screw was used to position the sample within a close proximity to the indenter. The moment of contact between sample and the indenter and the subsequent time dependence of the penetration depth, h(t), were monitored by a capacitance gauge. The signals from displacement sensor and the load cell were recorded by PC controlled Data Acquisition System, which allowed their synchronous registration within an accuracy of 25 μs. The displacement sensitivity and the time resolution were 1 nm and 50 μs, respectively. Loading and unloading indentation cycles were accomplished by programmable variation of electric current in the electromagnetic force transducer, with the duration of the whole cycle being varied from 0.1 ms to 300 sec. It enables generation of load pulses of different shapes (triangular, saw-tooth and square wave). Dependencies $F(h)$ for LiF and Si for different duration of a full loading-unloading cycle by a symmetric triangular force pulses are shown in Fig. 3 to illustrate the capabilities of our tester to conduct research of the dynamic nanohardness.

Under the action of a "rectangular" load pulse, generated by the electromagnetic force transducer (pulse leading edge duration ~0.1 ms), the shaft with the indenter advanced with a constant acceleration in the absence of a sample (Fig. 4), and without any delay from the moment of switched on current. This means that a steady force F_0 was indeed applied to the mobile

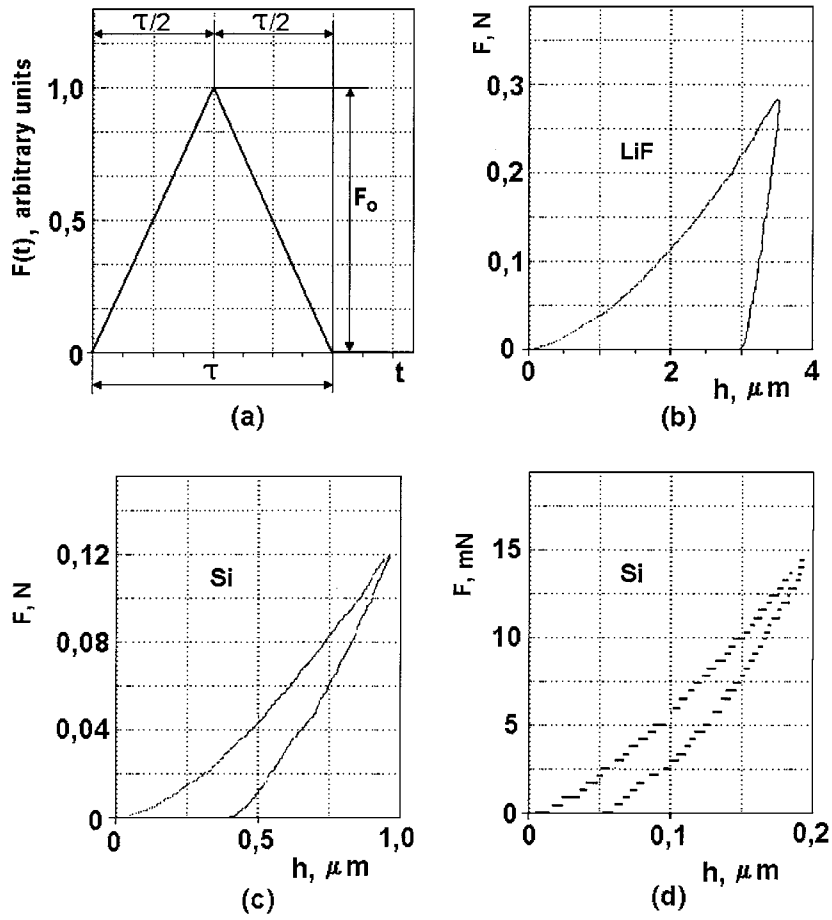

Figure 3 Shape of a loading pulse (a). Load - displacement curves for different duration τ and maximum load F_0 in two crystals: LiF, $T = 293$ K, $\tau = 10$ s (b); Si, $T = 293$ K, $\tau = 10$ s (c); Si, $T = 293$ K, $\tau = 50$ ms (d).

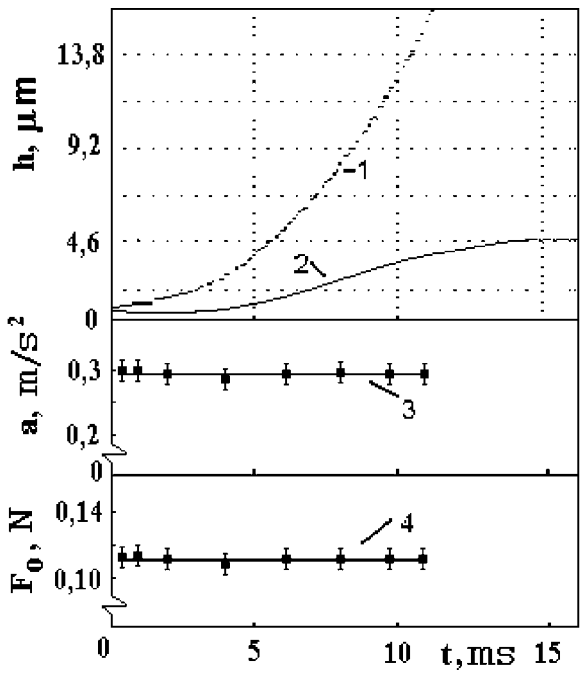

Figure 4 Time dependence of indenter displacement $h = f(t)$, 1: without a sample, 2: with a NaCl sample, 3: indenter acceleration $= \mathrm{d}^2h/\mathrm{d}t^2$, 4: $F = f(t)$ in the absence of the sample. =293.

parts of the tester (friction effect is negligible). Due to negligible friction effect, measured time dependencies of the indenter penetration depth into material, $h(t)$, (see for example, Figs 4 and 5) reflects dynamics of physical processes in the deformation zone and can be used for identification of atomic mechanisms of material displacement underneath the indenter. The same arguments can be used to interpret the time dependencies of resistance force of the material to indenter penetration $F(t)$: in these conditions it was also determined only by properties of sub-surface layers of the sample. Actual duration of the pulse leading edge $F(t)$ (i.e. the time required for the applied force to reach an amplitude value, close to the value of F_0 generated by the electromagnetic force transducer) constituted several ms (1–3 ms depending on the material and applied force).

To record the electrical signal induced by the formation and motion of charged structural defects underneath the indenter, the sample was placed between two identical probes. The potential difference from these probes was applied to the differential input of a broad - band (10^{-1}–10^6 Hz) amplifier with an input resistance of 10^{11} Ohm. This arrangement provided an opportunity to record the sample electric dipole momentum, $P(t)$, synchronously with the indenter penetration depth. It is well known, that in crystals with ionic or covalent bonds almost all of the structural defects (dislocations, impurity atoms, vacancies, etc.) carry an electric charge [18, 19]. Their displacement during mechanical loading leads to electrical polarization of the crystal. The dynamic dipole momentum, $P(t)$, as shown in [20, 21], is proportional to the quantity and displacements of moving charged defects. It provides an additional opportunity for the *in situ*

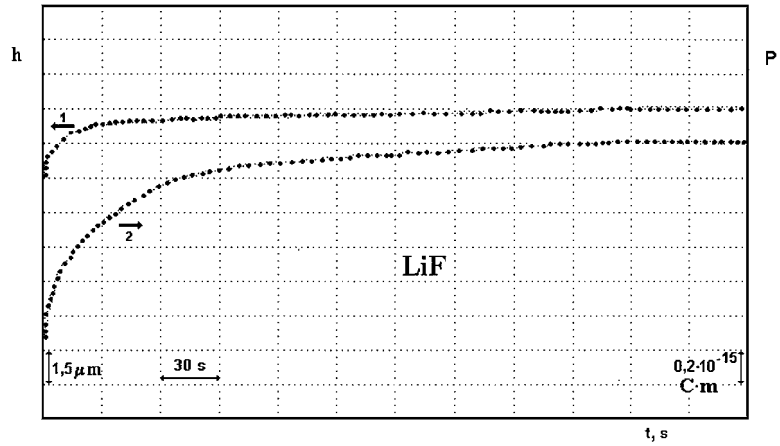

(a)

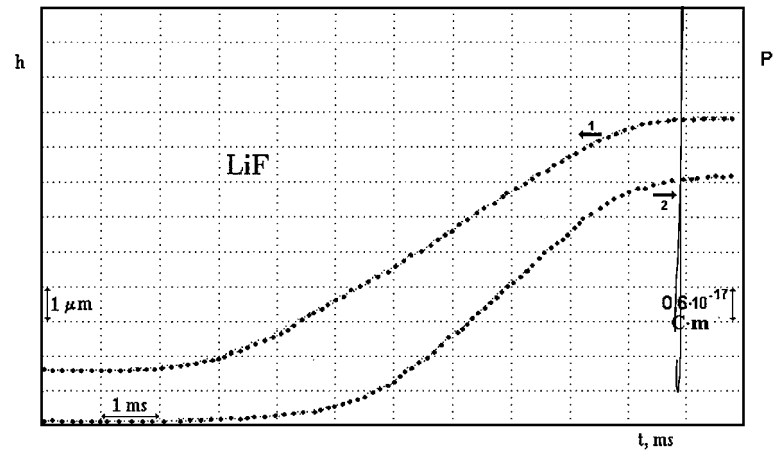

(b)

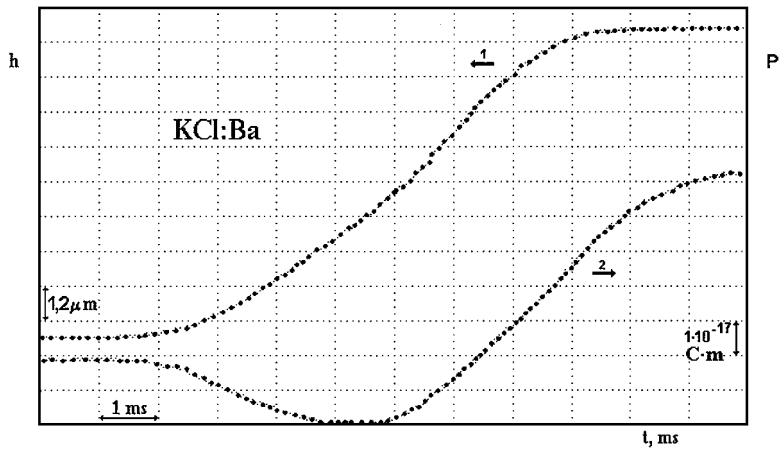

(c)

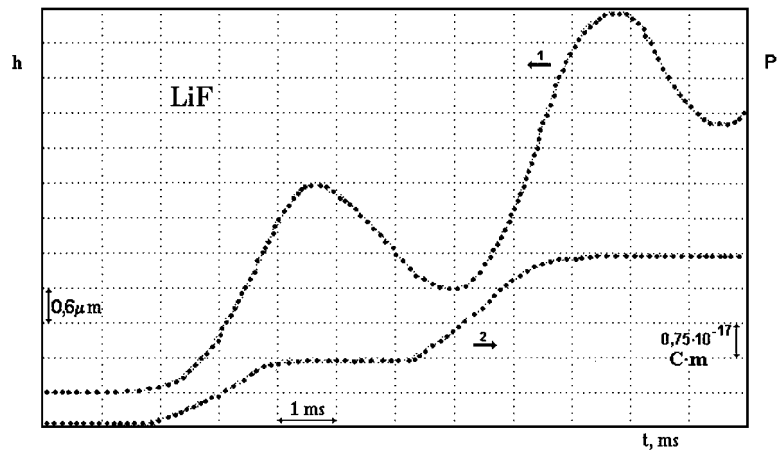

(d)

Figure 5 Time dependence of indenter penetration ($h(t) - 1$) and electric dipole momentum ($P(t)$- 2) for some ionic crystals: (a) LiF- $T = 293$ K; (b) LiF- $T = 293$ K; (c) KCl:Ba (0,1 mol% Ba) - T - 77 K; (d) LiF - T-77 K.

non-contact registration of the dynamics of micromechanical events. This information can be very useful for practical applications; as an example—it was shown in [22] that wear resistance of zirconia based ceramics correlates well with properties of the particular material to retain electrical charges injected into it. Another example—the amplitude and frequency spectrum of electrical signals, generated as a result of irradiation of NaCl, LiF and ZnS samples by high power beam of CO_2 – laser, is completely determined by the character of optical damages in the sub-surface layers and by a type of generated defects (rosette dislocations, cracks or fusion zones) [23].

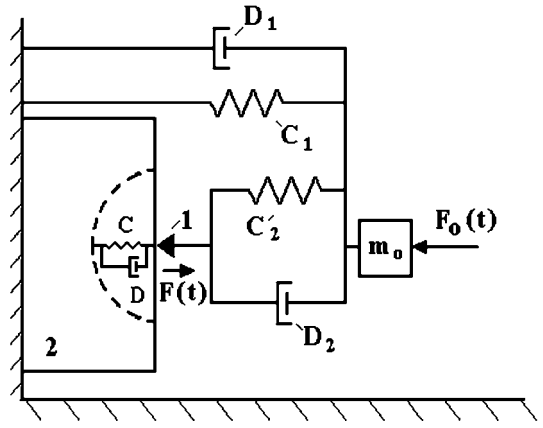

Figure 6 A model representation of an oscillating system. 1: indenter; 2: sample; m_0: mass of the movable part of load cell; C and D, C_1 and D_1; C_2 and D_2: stiffness and damping coefficients of the indentation zone, the suspension and the shaft respectively.

3. Results

Despite large differences in mechanical properties of investigated crystals (their Young's modulus differed more than an order of magnitude and hardness differed almost two orders of magnitude), the indenter penetration kinetics was qualitatively similar. $h(t)$ curves show typical s-shape behavior. Following initial 1–3 msec of activation time, $h(t)$ rapidly increased and attained 80–90% of its final value during 10–12 ms from the onset of displacement. During the same time, $P(t)$ reached 25–30% of their final values (see Fig. 5a) (except for MgO, Si and metals where polarization has not been detected). The depth, $h(t)$, reached its final values within 10 to 100 sec of loading, and $P(t)$ – within 10 to 300 sec. This duration depended on type of material studied, test temperature, and amplitude load. Generation of cracks, observed in optical microscope during unloading [24], was accompanied by abrupt changes in $P(t)$ with the duration of the pulse leading edge being $\sim 1\ \mu$s. The amplitudes of these jumps of both polarities were $\sim 10\%$ of the final signal amplitude, clearly distinguishing them from usually slow variations of $P(t)$ ($t_{90} > 10$–20 msec) which is typical for processes involving plastic deformation [20, 21, 24–26].

We noticed some peculiarities in the $P(t)$ behavior during initial stages of the indenter penetration. In all of the investigated ionic crystals we observed that activation time for $P(t)$ was from 1 to 4 msec longer than for $h(t)$ (see, Fig. 5b). This delay was slightly dependent on the temperature and the applied load. In contrast to all the crystals studied, $P(t)$ changed its polarity during indenter penetration in KCl:Ba (0.1 mol% Ba) crystals (Fig. 5c).

In a number of experiments, $h(t)$ showed damped oscillations (Fig. 5d). These oscillations were observed only in relatively hard materials (or during low temperature tests), provided that load pulse leading edge was shorter than 2 msec (MgO and Si at room temperature, LiF at $T \leq 200$ K, NaCl and K I at $T \leq 100$ K). Similar oscillations were observed in [13] during high rate indentation of In. Indentation of soft crystals (KCl, NaCl, LiF, Pb, and Al) at room temperature did not show oscillations. We demonstrated that these oscillations are not related to resonant frequency of the test apparatus but related to "indenter – contact zone". The dynamic model of the oscillatory system (Fig. 6) takes into account the mass of movable parts of the loading unit, m_0, the stiffness of the springs of suspensions C_1, the stiffness of the shaft C_2, the stiffness of the sample in the contact zone C, and the dissipative properties of these elements with corresponding coefficients of damping D_1, D_2 and D. The most complicated and important parameter is $C = kE_r A^{1/2}$, where k-is the proportionality coefficient depending on the shape of the indenter [5–7], $A = Gh^2$ is the projection of the contact area of the indentor, $E_r = [(1-\nu^2)E^{-1} + (1-\nu_i)E_i^{-1}]^{-1}$ is the effective Young's modulus, E and ν - are Young's modulus and Poisson's ratio for the sample material, E_i and ν_i - for the material of the indenter, respectively. Circular frequency of the natural damped oscillations ω is correlated with these parameters through the obvious equation $\omega = \{[(C^{-1} + C_2^{-1})^{-1} + C_1]m_0^{-1} - D^2\}^{1/2}$. Design details of the test apparatus were taken into acount to meet the following requirements: $C_2 \gg C$, $C_1 \ll C$, $D_1 \ll D$ and $D_2 \ll D$ (in our apparatus, $C_2 = 50$ MN/m, $C_1 = 1$ kN/m, $D_1 < 1$ s^{-1}, $D_2 < 0.1$ s^{-1}, $D \geq 30$ s^{-1} and the measured value of C was ≤ 1 MN/m). The regime of penetration and the arising oscillations, in the first approximation, depend only on the properties of the material in the contact zone, i.e. on C and D values. Increase in h results in the proportional growth of C. At some critical value h_c, the regime changes from a periodic to oscillatory due to Cm_0^{-1} exceeding D^2. These regime changes in our crystals occurred only at $h_c \approx 3$–$14\ \mu$m. The frequency of self-oscillations of the movable suspended mass was much lower than ω, and the frequency of self-oscillations of the shaft was much higher than ω. Therefore, these oscillations did not interfere with the measuring procedure.

Thus, the amplitude, frequency, and decay decrement of oscillations provides information on mechanical properties of material in the contact zone. Measurements of the parameters of self-oscillations in the "sample – indenter system can be used to calculate the Young's modulus in microvolumes (1–$10^3\ \mu$m^3).

Continuous registration of the penetration depth of the indenter vs time $h(t)$ allows estimation of instantaneous values:

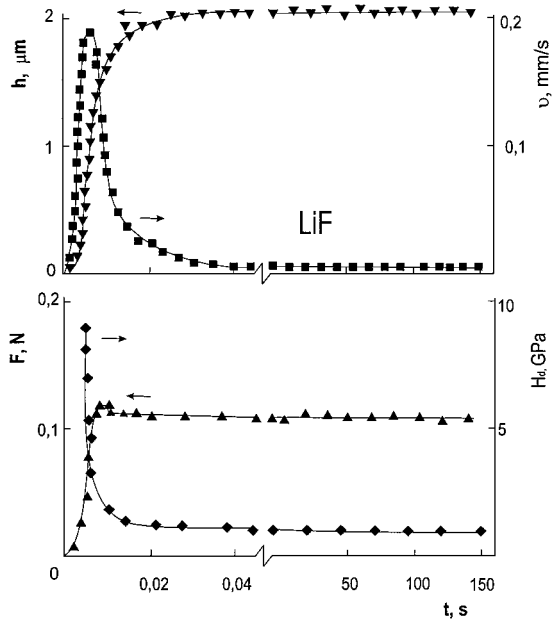

Figure 7 Time dependence of the indentor displacement $h = f(t)$, displacement velocity $\upsilon = \mathrm{d}h/\mathrm{d}t = f(t)$, applied load $F = f(t)$, dynamic hardness $H_\mathrm{d} = f(t)$ for (001) surface of LiF, at $T = 300$ K. Indention load - 0.11N.

i) linear velocity $\mathrm{v}(t) = \mathrm{d}h/\mathrm{d}t$;
ii) strain rate $\dot{\varepsilon}(t) = \mathrm{d}h/h\mathrm{d}t$;
iii) resistance force of the material to indenter penetration $F(t) = F_0 - m_0(\mathrm{d}^2h/\mathrm{d}t^2)$;
iv) averaged over the imprint area of contact stresses under the indenter $\sigma(t) = F(t)/A(t)$ or dynamic hardness by Meyer $H\mathrm{d}(t) = \sigma(t)$.

$F(t)$ can be measured independently by piezoelectric transducer (see Fig. 2).

Typical dynamic dependencies $\nu(t)$, $F(t)$, $H_\mathrm{d}(t)$ in case of LiF crystals are shown in Fig. 7. Accuracy of definition $\sigma(t)$ and $H_\mathrm{d}(t)$ at the initial stages ($h > 0.5$ μm) may be estimated as ~10–30%. However, with increasing values of h and A the estimation error of $\sigma(t)$ and $H_\mathrm{d}(t)$ decreased, and the resistance force $F(t)$ was asymptotically approaching a predetermined force F_0. In 5–7 ms from the onset of loading, a relative error in estimation of σ(t) and $H_\mathrm{d}(t)$ was ~ few percent. At $t \geq 1$s, H_d reaches the static value of hardness H_st determined independently by a traditional hardness tester.

Process of indenter penetration into investigated crystals consisted of as many as four distinct stages (instead of just two stages—fast and slow—, usually postulated so far). It can be seen from the kinetic curves of $\ell n\dot{\varepsilon} = f(t)$ and $\ell n\dot{P} = f(t)$ plotted in semi-log coordinates (Fig. 8). The strain rate decreases almost linearly in each stage, which suggests an exponential relaxation process. $\dot{\varepsilon} \sim \dot{\varepsilon}_\mathrm{o} \exp(-kt)$ [or $\dot{P} \sim \dot{P}_\mathrm{o} \exp(-k_1 t)$].

The differences in the k (k_1) values on different stages were as high as four orders of magnitude, and the differences in the pre-factor values ($\dot{\varepsilon}_\mathrm{o}$, $\dot{P}_\mathrm{o}$) were more then five orders of magnitude. These drastic differences in the quantitative description of $h(t)$ and $P(t)$ at different stages suggest changes in the rate controlling processes (presumably changes in the mass transfer mechanism

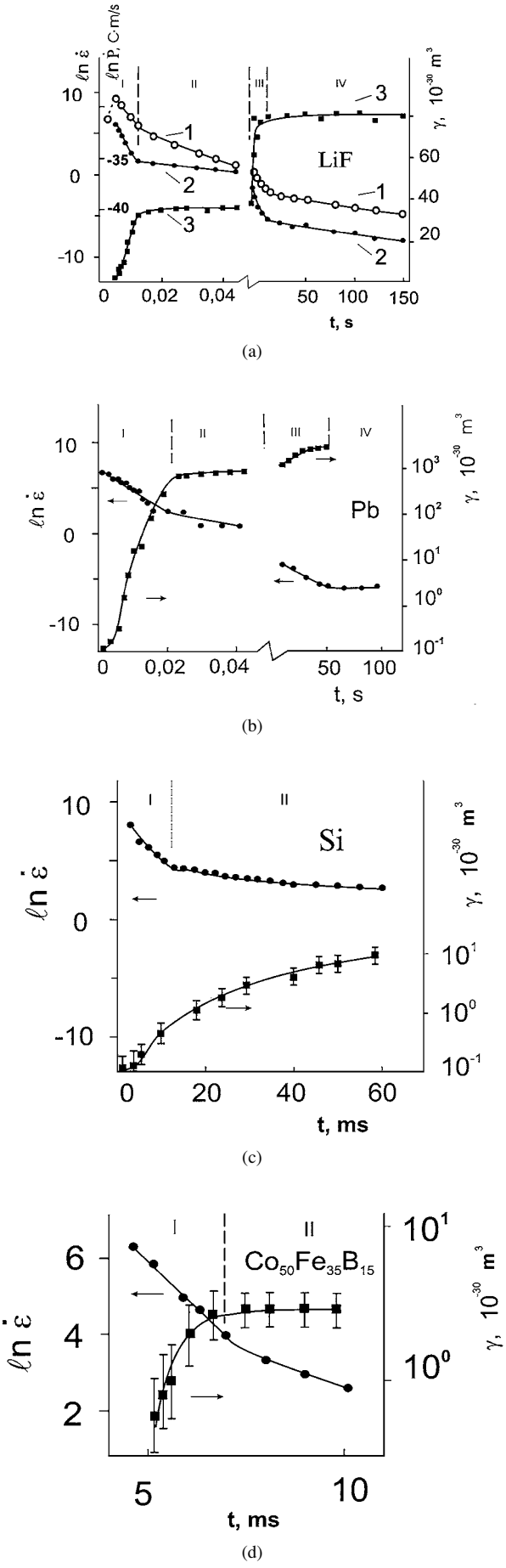

Figure 8 Time dependence of the strain rate ($\ell n\dot{\varepsilon} = f(t)$), dipole momentum $\ell n\dot{P} = f(t)$, and activation volume ($\gamma = f(t)$) (a) LiF (1 - $\ell n\dot{P} = f(t)$, 2 - $\ell n\dot{\varepsilon} = f(t)$; 3 - $\gamma = f(t)$; (b) Pb; (c) Si; (d) $o_{50}Fe_{35}B_{15}$. Stages of indentation are marked by Roman numerals: I – the first, II – the second, III – the third, IV – the forth.

in the contact zone). As seen from Fig. 8, rate dependencies of $\dot{\varepsilon}(t)$ and $\dot{P}(t)$ can be described by the same number of stages with a similar duration for each stage (despite obvious dissimilarities in the shape of $h(t)$ and $P(t)$ curves (see Fig. 5). These dissimilarities in the $h(t)$ and $P(t)$ curves provide an indirect prove that they contain an independent information and can not be explained by a trivial "dynamic capacitor" effect.

4. Discussion

"*in situ*" recording of indenter penetration dynamics provides a uinque opportunity to obtain valuable information about the sequence and the nature of the processes taking place underneath the indenter.

It should be mentioned, that despite a relatively low absolute indenter velocity (less than 1 mm/s, see Figs 5 and 7), small size of the deformation zone ($\approx h$) leads to very high apparent strain rates, ε, of the material underneath the indenter during initial stages of indentation (first few milliseconds). The maximum attainable strain rate is $\dot{\varepsilon} = \dot{h}/h \geq 10^2$ s^{-1}, which is comparable with a typical values for high-speed collisions between macroscopic bodies. It is a well-known that plasticity of even very soft crystals is greatly suppressed under these conditions. As a result, quasi-elastic deformation should dominate up till much larger loads, than it is usually observed during quasi-static process of nanoindentation [3, 27, 28]. Dynamic hardness during initial stages of indenter penetration exceeds several times (up to 10) the static one.

Fig. 9 shows that initial stages of the penetration velocity-force dependence can be described by a straight line. Extrapolation to $\sigma_0 = 0$ will provide an apparent velocity $\dot{\varepsilon}_0$ at the onset of plastic deformation. Temperature dependence of $\ell n\dot{\varepsilon}_0$ is shown in Fig. 10. Data can be described by an Arrhenius law $\dot{\varepsilon} = \dot{\varepsilon}_0 \exp(U - \gamma\sigma)$.

Activation volumes γ obtained from the slope of $\ell n\varepsilon$ vs $f(\sigma)$ at the initial stages of penetration have very low values $\sim 10^{-30}$ m^3 for all investigated materials (see Fig. 8). Corresponding activation energies—U—for ionic crystals were ~0.01–0.1 eV (depending on the temperature).

Apparent values for activation volumes as a fraction of a volume (V_c) occupied by an atom (cation) in the

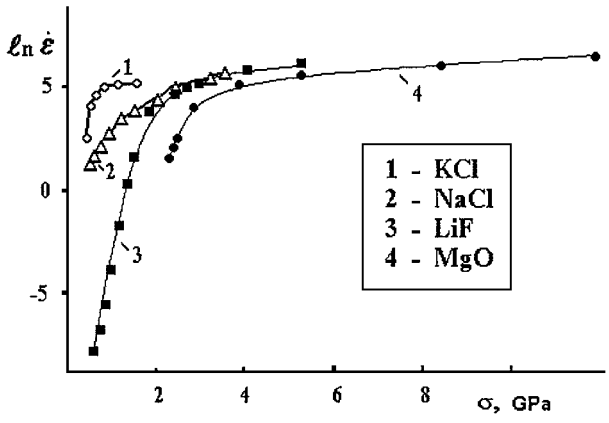

Figure 9 Stress dependence of the strain rate for ionic crystals: KCl - 1; NaCl - 2; LiF - 3; MgO - 4.

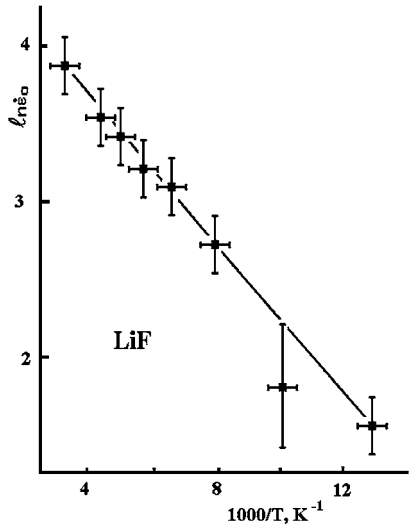

Figure 10 Temperature dependence of the strain rate for LiF crystals.

lattice at normal pressure implies that plastic deformation occur via motion of individual atoms. Effect of hydrostatic confining pressure on the diffusion rate also provides an estimate of γ as ~0.6–0.7 V_c. It should be mentioned that there are alternative diffusion related mechanisms of dislocation plasticity (dislocation climb for example), which are also characterized by small values of $\gamma \approx V_c$. However, at low temperatures used in our study they are too slow to sustain high strain rate $\dot{\varepsilon} \sim 10^3$ s^{-1} observed during initial stages of indenter penetration. Low activation volume and high strain rate at low indentation temperatures support earlier ideas on mass-transfer mechanisms via non-equilibrium point defects (interstitials or crowdions) [29–31].

As seen from Fig. 8, at later stages of indenter penetration ($t \geq 10 - 12$ ms), H_d approaches static value of microhardness H_{st}, U (in ionic crystals) increases up to values ~0.2–0.3 eV and γ - up to 10^{-28} m^3. For these indentation stages γ values become closer to $\sim 10\ b^3$ (where b – Burgers vector of glide dislocations). These values for activation volume are typical for dislocation mechanism of material flow underneath the indentor [8–11, 32, 33].

In [34, 35] binding and migration energies of interstitial clusters in some f.c.c. crystals were calculated by molecular dynamics simulations in a multi-particle potential. It was shown that such clusters are formed during $t \leq 10^{-11}$ s, with the formation energy for individual interstitial atom being ~ several eV. These clusters of interstitial atoms can move with very low activation energies ($\sim 10^{-2}$ eV) along directions of close packing, which can provide a very effective crowdion mechanism for mass transfer. As follows from the above discussion, our interpretation of experimental data are in agreement with the results of computer simulations [34, 35]. Apparently, high stress concentration at the initial stages of indenter penetration leads to generation of high density of non-equilibrium point defects (without thermal activation). Low values of U and γ during several first ms of penetration imply that subsequent displacement of these non-equilibrium point defects involves thermal activation.

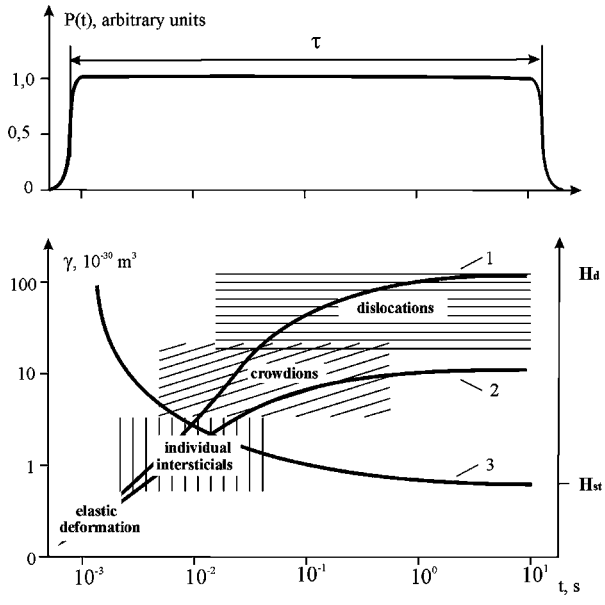

Figure 11 The scheme of deformation mechanisms change at print formation. 1: activational volume of γ for soft materials (Pb, NaCl, LiF); 2: activational volume γ for hard materials (Si, amorphous metal alloy $Co_{50}Fe_{35}B_{15}$); 3: dynamic microhardness H_d. $F(t)$: "rectangular" force pulse. H_{st}: quazistatic hardness.

Since in the above describe estimations of γ we did not take into account several factors, namely: elastic component of deformation, inhomogeneity of applied external stresses and an effect of internal stresses, the accuracy of γ assessments is not very high, specially during initial stages of indentation (10–30%). Despite relatively high error in γ estimations, certain distinctions between potential mechanisms involved in mass-transfer can be drawn from the available data. Differences in activation volumes between point defect's and dislocation-controlled processes of plastic deformation are usually 2–3 orders of magnitude [29]. This difference is far beyond uncertainty in our evaluations of γ. A schematic diagram representing transitions between dominating mechanisms of plastic deformation during residual impression formation is shown in Fig. 11.

There are numerous independent experimental evidences of generation and motion of high concentration of non-equilibrium point defects during indentation [36–42]. However, reliable quantitative information regarding non-equilibrium point defect concentration and their mobility is still lacking.

We used results obtained in the present work to provide quantitative information regarding relative contributions of non-equilibrium point defects and dislocations in the displacement of material's volume during residual impression formation [43]. We assumed that for activation volumes $\gamma_p \leq 10 \times 10^{-30}$ m^3 plastic deformation is defined by point defects and their clusters, and for $\gamma_p \geq 50 \times 10^{-30}$ m^3 it is defined by dislocation plasticity. Then from the loading part of the indentation curve we determined values of h_i corresponding to a transition in the mechanisms of plastic deformation. For indenter penetration distance (h_i), we estimated displaced material volume as $V_i = (49/6) \times (h_i)^3$ and normalized this volume by the displaced material volume at the maximum penetration (h_{max}), which provided us with a relative contribution of point defects and dislocations in residual impression formation. Results of these estimations for different materials are shown in Table I. This approach does not take into account elastic recovery during unloading (see Fig. 3). However, elastic recovery for soft crystals was small (see Fig. 3b) and does not significantly affect ratio of point defects/dislocations related volumes. For hard crystals (see Fig. 3c) dislocation plasticity was insignificant and almost 100% of the displaced volume can be attributed to point defects.

Data shown in Table I clearly indicate that for all investigated materials even for relatively long indentation duration ($\tau \geq 1$ s) considerable part of plastic deformation and mass-transfer in the vicinity of indenter imprint can be attributed to point defects (individual atoms or small clusters of them). During initial stages of indentation ($\tau \leq 10$ ms) role of dislocation plasticity in mass-transfer underneath the indenter diminishes significantly and hardly exceeds 10% even in soft crystals. During initial indentation stages with prevailing effect of point defects over dislocation plasticity, dynamic hardness H_d can significantly exceed its static values H_{st} (see Table I).

Additional valuable information regarding mechanism of mass transfer during indentation can be obtained from kinetic of electrical polarization in the vicinity of indenter impression. In alkali halides crystals (NaCl, KCl and LiF) slightly doped with low level of aliovalent impurities ($\sim 10^{-3}$ at%), sing and amplitude of P at saturation agree well with the charge sign and density of dislocations propagating from the

TABLE I

Materials	Indentation load N	$\frac{H_d^{max}}{H_{st}}$	Contribution of point defects		Contribution of dislocations	
			$\Delta h_i/h_k$	$\Delta V_i/V_o$	$\Delta h_i/h_k$	$\Delta V_i/V_o$
KCl	0.11	5	0.7	0.34	0.10	0.24
NaCl	0.11	7	0.69	0.33	0.17	0.42
LiF	0.11	9	0.64	0.26	0.1	0.25
MgO	6.0	10	0.68	0.31	–	–
Pb	0.25	3	0.46	0.10	0.42	0.80
Al	0.25	9	0.58	0.20	0.33	0.70
$Co_{50}Fe_{35}B_{15}$	0.25	10	1.00	1.00	0	0
Ge	2.3	10	0.67	0.30	0.26	0.6
GaAs	3.8	10	0.49	0.12	0.4	0.78

indenter impression into the crystal bulk. Preliminary plastic deformation of a sample up to $\varepsilon \sim 10\%$ has very little effect on hardness, however, it significantly affect dislocation mobility and P. During indentation of LiF we observed that steep increase of $P(t)$ was delayed for ~2–4 ms relative to $h(t)$ (see Fig. 5b). Duration of this activation time correlates well with the duration of the initial, non-dislocation stage of mass-transfer. During initial stage of indentation in KCl crystals heavily doped with Ba (up to ~0.1%), instead of activation time we observed polarization signal, which is opposite to the polarity expected from dislocation plasticity (see Fig. 5c). In 5–7 ms, sign of P changed to "normal" for dislocation plasticity. This interesting effect can be explained assuming that initial stages of polarization are caused by displacement of intrinsic cation interstitials enhanced by high concentration of charge compensating vacancies. Thus sign inversion of P in heavily doped crystals is related with a change in dominating carriers of plastic deformation carring opposite electrical charge. Cations transport "plus" sign, but dislocations - "minus" sign.

From the above discussion it follows that impact of point defects should be more pronounced at low h. It is also well known from simple geometrical consideration that hardness $H \sim 1/h^2$ and displaced volume $V \sim h^3$. Thus for low h one can expect more pronounced effect of point defects on hardness than on displaced volume. Relative contribution of dislocation plasticity for low h is relatively small, thus changes in dislocation density and mobility cannot result in proportional changes in hardness. Relatively poor sensitivity of hardness to conditions of dislocation generation and motion was indeed observed.

We believe that above discussion is important not only for deeper understanding of basic mechanisms of plastic deformation and mass transfer during indentation, but may find far reaching practical implications. We demonstrated that non-equilibrium point defects play an important role in material's property known as hardness. This information provides a new insight on different ways for optimization of wear resistance of structural materials.

5. Conclusion

1. A new technique for investigation of elastic and plastic properties of materials and the dynamics of structural defects in micro-volumes, $\sim \mu m^3$, was developed. The technique is based on the analysis of the kinetics of the indenter penetration into a material surface as a result of quasi instantaneous load application.

2. The apparatus and the technique developed provides an opportunity to study dynamics of the indenter penetration with the highest time resolution (~ 50 μs) attained so far for displacement sensitive indentation testers. The experimental apparatus was also capable of recording electrical polarization of the indentation zone with a time resolution of ~ 0.1 μs in crystals containing charged structural defects.

3. Dynamics of indenter penetration is described by Arrhenius law. It is shown that penetration process consists of several stages (as many as four in some cases) differing in activation volume and activation energy. A model is proposed describing dominating mechanisms of plastic deformation and mass-transfer at each stage. Based on the analysis of activation parameters, it is shown that the residual impression formation involves the following stages:

a) elastic deformation of the material;
b) plastic deformation via generation and displacement of non-equilibrium individual point defects and then their clusters (crowdions);
c) dislocation plasticity.

4. Relative role of different plastic deformation mechanisms is evaluated, and it is shown that even in soft crystals, point defects play an important role in microhardness. In hard materials (for instance, Si, amorphous alloys) and short indentation times, the residual impression formation and hardness is mostly defined by non-dislocation plasticity.

Acknowledgment

The work was supported by the Russian Foundation for Basic Research (Project Code 98-02-16549).

References

1. V. P. ALEKHIN, G. S. BERLIN, A . V. ISAEV, G . N. KALEI, V. A. MERKULOV, V. N. SKVORTSOV, A. P. TERNOVSKII, M. M. KRUSHCHOV, G. D. SHNYREV and M. KH. SHORSHOROV, *Industrial Laboratory* **38** (1972) 619.
2. S. I. BULYCHEV, V. P. ALEKHIN, M. KH. SHORSHOROV, A. P. TERNOVSKII and G. D. SHNYREV, *ibid.* **41** (1975) 1409.
3. W. C. OLIVER and C. J. MCHARGUE, *J. Mater. Res.* **7** (1992) 450.
4. S. V. HAINSWORTH and T. F. PAGE, *J. Mater. Sci.* **29** (1994) 5529.
5. W. C. OLIVER and G. M. PHARR, *J. Mater. Res.* **7** (1992) 1564.
6. G. M. PHARR, W. C. OLIVER and F. R. BROTZEN, *ibid.* **7** (1992) 613.
7. Y. MURAKAMI, K. TANAKA, M. ITOKAZU and A. SHIMAMOTO, *Phil. Mag. (A).* **69** (1994) 1131.
8. M. S. KATS and V. R. REGEL, *Fiz. Met. Metalloved.* **40** (1975) 612 (Phys. Met. Metallogr).
9. S. N. G. CHU and J. C. M. LI, *J. Mater. Sci.* **12** (1977) 2200.
10. YU. C. EDWARD and J. C. M. LI, *Phil. Mag.* **36** (1977) 811.
11. S. N. G. CHU and J. C. M. LI, *Mater. Sci. and Engineer.* **39** (1979) 1.
12. M. YOSHIOKA and N. YOSHIOKA, *J. Appl. Phys.* **78** (1995) 3431.
13. B. N. LUCAS and W. C. OLIVER, *Mat. Res. Soc. Proc.* **358** (1995) 645.
14. Z. GYULAI and D. YARTLY, *Z. Phys.* **51** (1928) 378.
15. A. V. STEPANOV, *Z. Phys. Bd.* **81** (1933) 560.
16. YU. I. GOLOVIN, V. I. IVOLGIN, V. V. KORENKOV and A. I. TYURIN, *Pis'ma Zh. Techn. Fiz.* **23** (1997) 15 (JTP Lett).
17. *Idem., Zh. Techn. Fiz.* **70** (2000) 82 (JTP).
18. R. W. WHITWORTH, *Advances in Physics* **24** (1975) 203.
19. V. F. PETRENKO and R. W. WHITWORTH, *Phil. Mag.* (A) **41** (1980) 681.
20. YU. I. GOLOVIN and A. I. TYURIN, *Izv. Akad. Nauk. Russia, Ser. Fiz.* **59** (1995) 49 [*Bull. Russ. Acad. Sciences (Physics).* **59** (1995) 49].

21. YU. I. GOLOVIN and A. A. SHIBKOV, *Kristallografiya* **35** (1990) 440 [*Sov. Phys. Crystallogr.* **35** (1990) 440].
22. A. MEDEVIELLE, F. THEVENOT and D. TREHEUX, *Wear* **213** (1997) 13.
23. YU. I. GOLOVIN, A. V. GORBUNOV and A. A. SHIBKOV, *Fiz. Tverd. Tela* (Leningrad) **30** (1988) 1931 [*Sov. Phys. Solid State* **30** (1988) 1931].
24. YU. I. GOLOVIN, A. A. SHIBKOV, A. I. TYURIN, YU. S. BOYARSKAYA and M. S. KATS, *ibid.* (Leningrad) **30** (1988) 3491 [*Sov. Phys. Solid State* **30** (1988) 3491].
25. YU. S. BOYARSKAYA, YU. I. GOLOVIN, M. S. KATS, A. A. SHIBKOV and A. I. TYURIN, *Phys. Stat. Sol.* (a) **130** (1992) 319.
26. YU. I. GOLOVIN and A. I. TYURIN, *Kristallografiya* **40** (1995) 884 [*Sov. Phys. Crystallogr.* **40** (1995) 884].
27. A. SHIMAMOTO and K. TANAKA, *Rev. Sci. Instr.* **68** (1997) 3494.
28. W. W. GERBERICH, W. YU, D. KRAMER, A. STROJNY, D. BAHR, E. LILLEODDEN and J. NELSON, *J. Mater. Res.* **13** (1998) 421.
29. V. L. INDENBOM and A. N. ORLOV, *Fiz. Met. Metalloved.* **43** (1977) 469 (*Phys. Met. Metallogr*).
30. V. L. INDENBOM, *Pis'ma Zh. Eksp. i Teor. Fiz.* **36** (1970) 526 [*JETP Lett.* **12** (1970) 526].
31. YU. I. GOLOVIN and A. I. TYURIN, *ibid.* **60** (1994) 722 [JETP Lett. **60** (1994) 722].
32. YU. S. BOYARSKAYA, D. Z. GRABKO and M. S. KATZ, "Physics of Microindentation Processes" (Kichineu, Shtiintsa, 1986) 322 p. (in Russian).
33. D. S. STONE and K. B. YODER, *J. Mater. Res.* **9** (1994) 2524.
34. P. ZHAO and Y. SHIMOMURA, *Computation Materials Science* **14** (1999) 84.
35. M. KOYANAGI *et al.*, *ibid.* **14** (1999) 103.
36. V. N. ROZHANSKII and M. A. VELEDNITSKAYA, *Phys. Stat. Sol.* (A). **8** (1971) 551.
37. V. N. ROZHANSKII, N. L. SIZOVA and N. L. URUSOVSKAYA, *Fiz. Tverd. Tela* (Leningrad) **13** (1971) 411 [*Sov. Phys. Solid State* **13** (1971) 411].
38. M. A. VELEDNITSKAYA, V. N. ROZHANSKII and L. F. COMOLOVA, *et al. Phys. Stat. Sol.* (a) **32** (1975) 123.
39. M. SH. AKCHURIN and V. R. REGEL, *Chemistry Reviews.* **23** (1998) 61.
40. M. SH. AKCHURIN, E. N. VASEV, E. YU . MIHINA and V. R. REGEL, *Fiz. Tverd. Tela* (Leningrad) **30** (1988) 760 [*Sov. Phys. Solid State* **30** (1988) 760].
41. B. YA. FARBER, V. I. ORLOV, V. I. NIKITENKO and A. H. HEUER, *Phil. Mag.* (A) **78** (1998) 671.
42. B. YA. FARBER, V. I. ORLOV and A. H. HEUER, *Phys. Stat. Sol.* (a) **166** (1998) 115.
43. YU. I. GOLOVIN and A. I. TYURIN, *Fiz. Tverd. Tela* (Sankt Peterburg) **42** (2000) 1818 [*Sov. Phys. Solid State* **42** (2000) 1818].

Received 30 May 1997
and accepted 21 February 2001